Long-term joint distribution of environmental conditions in a Norwegian fjord for design of floating bridges

Zhengshun Cheng[a,b,*], Erik Svangstu[c], Torgeir Moan[a], Zhen Gao[a]

[a] *Department of Marine Technology and Centre for Autonomous Marine Operations and Systems (AMOS), Norwegian University of Science and Technology (NTNU), Trondheim, 7491, Norway*
[b] *State Key Laboratory of Ocean Engineering, Shanghai Jiao Tong University, Shanghai, 200240, China*
[c] *Norwegian Public Roads Administration, Leikanger, 6863, Norway*

Abstract

A floating bridge is an attractive solution for crossing wide and deep fjords. To design a reliable and cost-effective floating bridge, it is very important to accurately evaluate the long-term environmental conditions at the local site in a fjord or strait, because it is relevant for the ultimate- and fatigue-limit state design check of floating bridges. This study addresses the long-term joint distribution of environmental conditions in a Norwegian fjord for design of floating bridges based on simulated wind and wave data from 2002 to 2017. The accuracy of simulated wave data is validated by comparison against field measurements. The joint distribution is established in terms of mean wind speed U_w, significant wave height H_s and peak period T_p, by assuming sequential stationary short-term conditions with a duration of one hour. The 100-year contour surface of wind and wave parameters is achieved, on which design points are suggested for long-term extreme response analysis by using the environmental contour method. Compared to joint distributions for open seas, the joint distribution in a fjord has fairly close values for environmental conditions with maximum U_w and with maximum H_s, which implies that fewer design points are required for the prediction of extreme responses.

Keywords: long-term joint distribution, wind and wave, contour surface, numerical simulation, field measurement

1. Introduction

Floating bridges are an attractive solution to improve the efficiency of crossing wide and deep straits or fjords. Although floating bridges have a very long history, traced back to 2000

*Corresponding author.
Email address: zhengshun.cheng@gmail.com

BC (Watanabe, 2003), their applications in modern infrastructure started around 1940. The first pontoon-type floating bridge was implemented in the Hobart Bridge, Australia in 1943. A worldwide development of floating bridges was reviewed by Watanabe (2003) and Kvåle (2017). Currently, several floating bridges are in operation, including four in the state of Washington in the USA and two in Norway. Moreover, Norway is currently running the Coastal-Highway Route E39 project, in which ferry transport across 8 fjords are to be replaced by bridges or tunnels. The width of these fjord crossings is up to 6km and the water depth is up to 1300m. Several innovative floating bridge concepts have been proposed (Eidem, 2017) and are being studied (Cheng et al., 2018; Fredriksen et al., 2019; Xu et al., 2018).

The safety of offshore structures is ensured by fulfilling limiting state design criteria. These limit states include fatigue-, ultimate-, and accidental-limit state (FLS, ULS, ALS) (Naess and Moan, 2013). The ULS design check of offshore structures is commonly based on environmental load effects corresponding to N-year (e.g., 100-year) wind and wave conditions. The long-term variation in wind and wave conditions is usually expressed in terms of mean wind speed, significant wave height, and peak period, by assuming sequential stationary short-term conditions with a duration, e.g., 1 hour. To obtain the long-term load effects that are relevant for ULS design check, the most accurate approach is to carry out a full long-term analysis, in which all environmental conditions are taken into account with consideration of their probability of occurrence. Nevertheless, this process requires massive computational efforts, which make the full long-term analysis impractical in engineering practice.

Approximate methods are thus proposed for estimating long-term load effects. A commonly used approach is the environmental contour method, in which the long-term extreme response for a return period of N-year is approximated by exposing the structure to a short-term extreme sea state (Winterstein et al., 1993; Haver and Winterstein, 2009). In particular, the sea state that leads to the largest short-term extreme responses is chosen from the N-year contour surface (or contour line when two environmental variables are present). In this case, the variability of the short-term extreme response should also be taken into account by multiplying a correction factor of 1.1-1.3 (Winterstein and Engebretsen, 1998), or by calculating the short-term extreme response at a higher quantile of 75-90% (DNV GL, 2014; NORSOK N-003, 2017), rather than 50%. In this approach, the N-year contour surface is derived from a long-term joint distribution of relevant environmental parameters, which is constructed based on the long-term variation of wind and wave conditions.

Construction of the long-term joint distribution of environmental parameters requires a large long-term dataset in order to reduce statistical uncertainties. To achieve an accurate prediction of extreme conditions, it was recommended by Bitner-Gregersen (2012) to use a dataset for over ten years to develop a joint environmental model. Moreover, since the numerically simulated data

of the most extreme wind and wave events are limited, it is important that the data are smoothed by fitting analytical distributions. To date, several joint distributions of environmental conditions have been established by fitting analytical distributions to raw data from field measurements at actual area (Johannessen et al., 2002; DNV GL, 2014) or from a numerical hindcast model (Li et al., 2015). These joint environmental models are developed for open seas. However, few studies on the development of the long-term joint distribution of environmental conditions in a fjord or strait have been conducted. The environmental conditions in a fjord or strait are different from those in the oceans. The present study deals with wave conditions in the Bjørnafjord. Compared to ocean waves consisting of wind waves and swells, the waves in a fjord can be dominated by wind-generated waves (Cheng et al., 2019b) due to limited fetch lengths. Therefore, the long-term joint environmental model in a fjord or strait is likely to differ from that in the open seas.

To establish the long-term environmental model in a fjord or strait, the wind and wave conditions at the local site should be accurately modeled. However, accurate modeling of long-term wind and wave conditions in a fjord or strait is very challenging, because of the complex topography and hydrography. The wind and wave conditions at the local site in a fjord or strait is usually achieved by numerical simulations based on hindcast data. In coastal regions, the SWAN (Simulating Waves Nearshore) model (Booij et al., 1999) is usually used to simulate the complex wave transformation caused by the bathymetry, wind and other factors. With respect to the local wind conditions, it is usually modeled by the Weather Research and Forecasting (WRF) model (Skamarock et al., 2008), which is a numerical weather prediction (NWP) system designed to serve both atmospheric research and operational forecasting needs.

The long-term environmental model is constructed based on stationary short-term conditions, in which the wind and wave conditions have identical duration. However, normally wind in 10 minutes and waves in 3 hours are considered as stationary. A compromise is usually a duration of 1 hour for both wind and waves. This is also used in the present study.

In this study, the long-term joint distribution of wind and wave conditions in a Norwegian fjord, i.e., the Bjørnafjord, is established based on numerically simulated wind and wave data over about 16 years. The simulated wave data is validated by comparison with field measurement. The developed joint environmental model can facilitate the ULS design check of floating bridges, by using the environmental contour method described above.

2. Data description

The Bjørnafjord is located at the Hordaland County, Norway. It has a width of approximately 4600m and a depth of more than 500m. The location and topography around the Bjørnafjord is depicted in Fig. 1. A floating bridge is planned for crossing the fjord. To design a reliable and

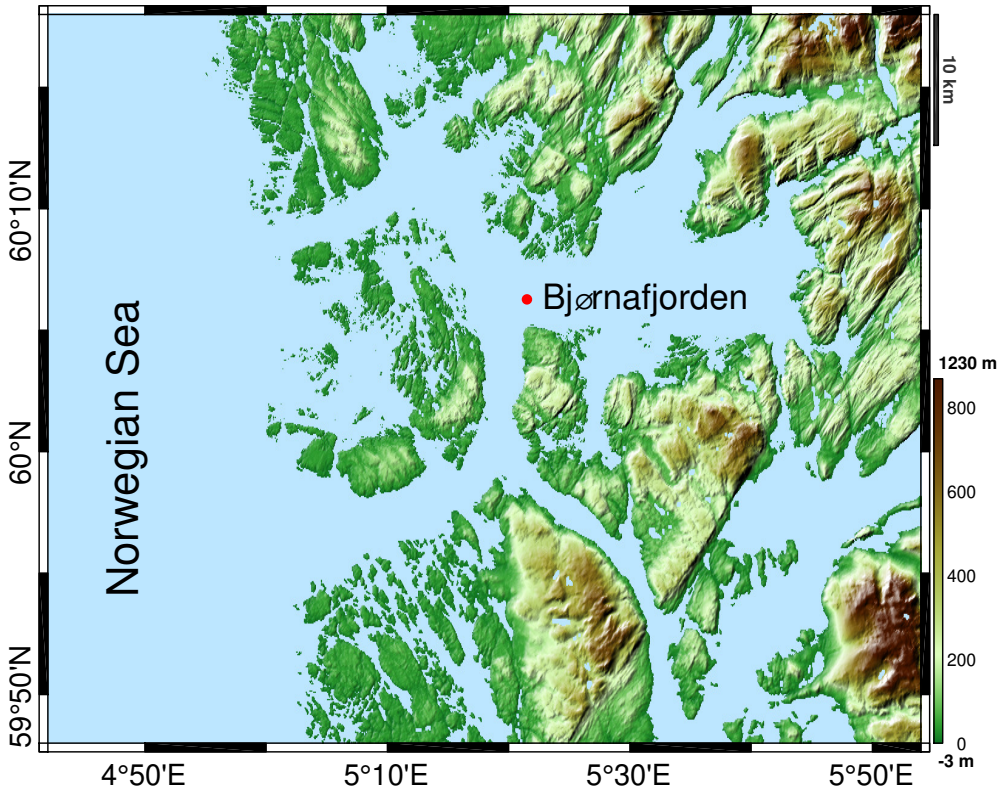

Figure 1: Location and topography of the Bjørnafjord. A Datawell waverider (DWR), marked as red point, was located in the fjord and its mean position is about 60°06′14.0″N and 5°21′34.9″E. This DWR corresponds to DWR3 shown in Cheng et al. (2019b).

cost-effective floating bridge, the environmental condition plays a vital role and should be properly evaluated.

To characterize the environmental condition in the Bjørnafjord, both numerical simulations and field measurements have been conducted. Currently, limited field measurements have been made. It is thus more feasible to construct the long-term joint distribution of environmental conditions in the fjord by using numerical simulations based on hindcast data. The field measured data is used to validate the accuracy of numerically simulated environmental data.

2.1. Field measurements of wave conditions

Field measurements of wave conditions were carried out by deploying three Datawell waveriders (DWRs) in the Bjørnafjord. The DWR records the heave, north and west displacements of the buoy in order to analyze the local wave condition. Principle on how the DWR measures wave condition is described in Datawell (2014) and by Cheng et al. (2019b) and is not presented in detail here.

The measurements have been performed since February 2016. The data are recorded in 30

minutes samples with a frequency of 1.28Hz. By analyzing the wave data measured from February 2016 to October 2017, Cheng et al. (2019b) identified the main characteristics of the measured wave condition. It was shown that the waves in the fjord are short-crested and mainly wind-generated. Swell might exist when waves come from northwest, but swell is very small. Waves with a small significant wave height ($H_s < 0.3$m) are likely to have multiple dominant directions, while waves with a relatively large significant wave height are likely to have one dominant direction.

It should be noted that there are two ferry routes crossing the fjord. The passing ferries generate ship waves, which are also recorded by the DWRs. Cheng et al. (2019b) proposed a band-pass filter based on wavelet and inverse wavelet analyses to detect and remove ship waves from raw data and concluded that the effect of ship waves is less important in cases with a higher significant wave height ($H_s > 0.3$m). Since waves with large significant wave height are of interest from design point of view, the raw data without removing ship waves are thus used for analyses in this study.

For the present study, a total of about 33 months (from February 2016 to October 2018) of measured data has been acquired. To validate the numerical simulations, wave measurement by only one DWR, denoted by DWR3 as shown in Fig. 1, is considered. The DWR is located in the middle of the fjord. The measured raw data are post-processed to achieve the wave data in every hour. The time history of measured significant wave height is shown in Fig. 2.

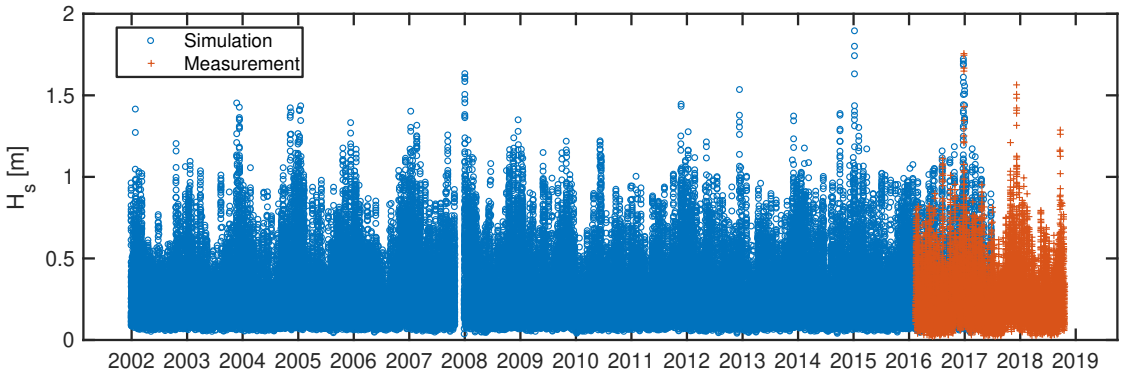

Figure 2: Time series of measured and simulated significant wave height at DWR3.

2.2. Numerical simulation of wind and wave conditions

The wind and wave conditions in the fjord are numerically simulated by using the SWAN (Simulating Waves Nearshore) model (Booij et al., 1999) and the WRF (Weather Research and Forecasting) model (Skamarock et al., 2008) in this study. The simulated wind and wave data are provided by the NPRA.

The SWAN model is a third-generation wave model for simulating realistic estimates of wave parameters in coastal areas, lakes and estuaries from given wind, bottom and current conditions.

The model is based on the wave action balance equation with sources and sinks, and solves the action density balance equation in time space, geographical space and spectral space. It can simulate wind-generated waves and swells at any scale relevant for wind-generated surface gravity waves. It can provide wave-frequency spectrum and directional spectrum, and accordingly wave parameters such as significant wave height, peak period, mean direction can be estimated; however, it cannot provide cross spectrum between different points because it is a phase-averaged model. In the numerical simulation, only wind-generated waves are considered. A total of 296×373 grid points are equally distributed in the area with latitude ranging from 59.85 to 60.2483 and longitude ranging from 4.8 to 5.797. The spacing between neighboring points is about 150m. Actually for the Bjørnafjord considered, wind-generated waves and swell were simulated separately, and swell data were simulated and analyzed by the Norconsult (Lothe and Musch, 2015).

The WRF Model is a next-generation mesoscale numerical weather prediction system designed for both atmospheric research and operational forecasting applications. It solves the compressible, nonhydrostatic Euler equations in the time and geographical spaces. It can be used for a wide range of meteorological applications across scales from tens of meters to thousands of kilometers. It provides the mean wind speed at 10m height for each grid point in the latitude and longitude directions, respectively. In the numerical simulation, 138×180 grid points are equally generated for simulating mean wind speed. The spacing between neighboring points is about 500m.

Numerical simulation of wind and wave conditions in the fjord are based on hindcast data from January 2002 to June 2017. During the numerical simulation, wave parameters (significant wave height, peak period, and mean direction) and wind parameters (mean wind speed in the latitude and longitude directions) are stored for each hour. Fig. 3 shows the spatial distribution of the significant wave height simulated by the SWAN model and the mean wind speed simulated by the WRF model during a storm condition in December 26, 2016.

In addition, since the mean position of the DWR3 is known from the field measurement, the wind and wave parameters at the location of DWR3 are interpolated and extracted from the simulated data. The significant wave height from numerical simulation at DWR3 is shown in Fig. 2. Herein, the extracted wind and wave parameters at DWR3 are used to construct the long-term joint distribution of environmental conditions in the fjord.

3. Validation of numerically simulated data

In this section, the simulated wave parameter at the location of DWR3 is compared with the measured wave parameter to validate the accuracy of numerical simulations. The simulated data and the measured data have an overlap from February 2016 to June 2017, about 17 months. Data during this period, in particular significant wave height H_s, is analyzed in depth to check the quality

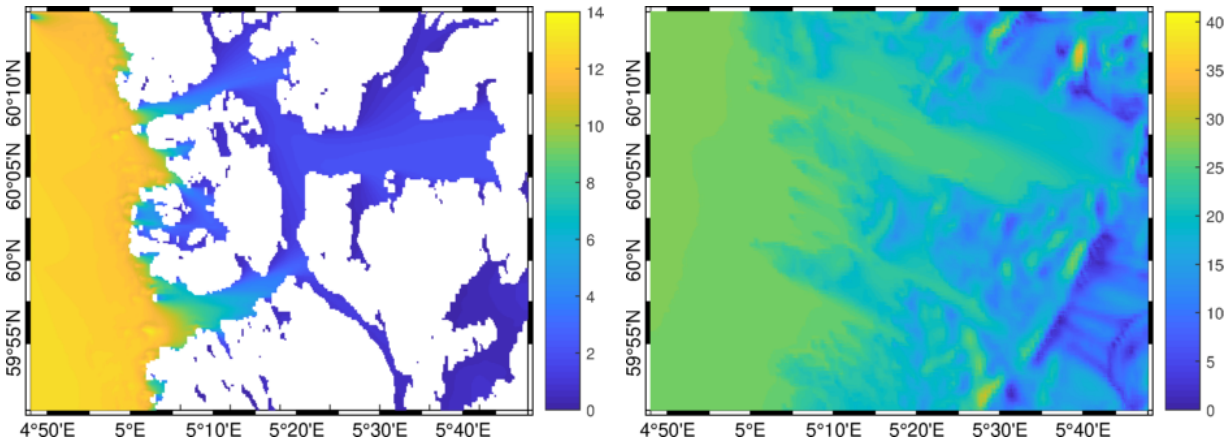

(a) Significant wave height (b) Mean wind speed

Figure 3: Distribution of simulated significant wave height and corresponding simulated mean wind speed in the Bjørnafjord during a storm condition on December 26, 2016.

of numerically simulated data.

Comparison of the field measured and numerically simulated significant wave height during this period is shown in Fig. 4. A close-up view of the time series of significant wave height during a storm condition is demonstrated in Fig. 5. It can be found that the simulated H_s has an overall good agreement with the measured H_s. The storm event during December 26, 2016 is well captured by the numerical simulation.

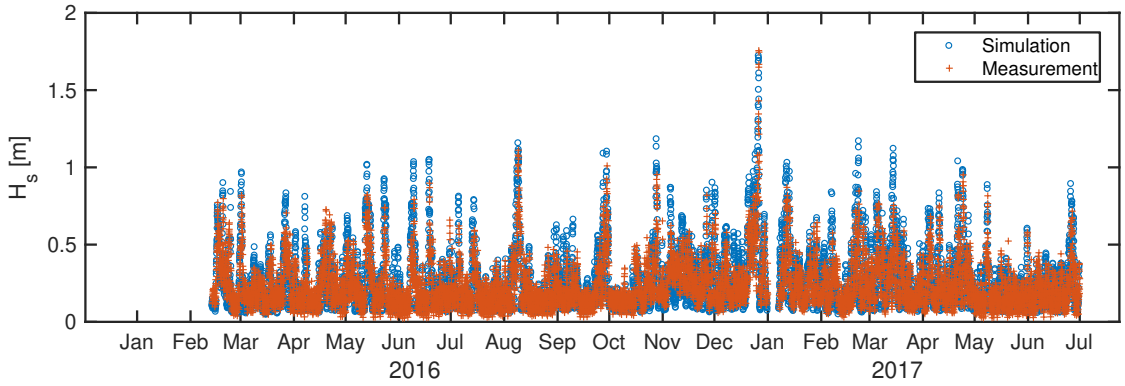

Figure 4: Comparison of time series of measured and simulated significant wave height at DWR3 from February 2016 to June 2017.

However, a small discrepancy between the simulated H_s and measured H_s, denoted by $\Delta H_s = H_{s,S} - H_{s,M}$, is also clearly observed from Figs. 4 and 5. A scatter plot of simulated and measured H_s is shown in Fig. 6. The regression line for simulated H_s larger than 0.3m has a slope of about 0.716. For simulated H_s larger than 1.2m, the simulated and measured H_s, marked by red + in

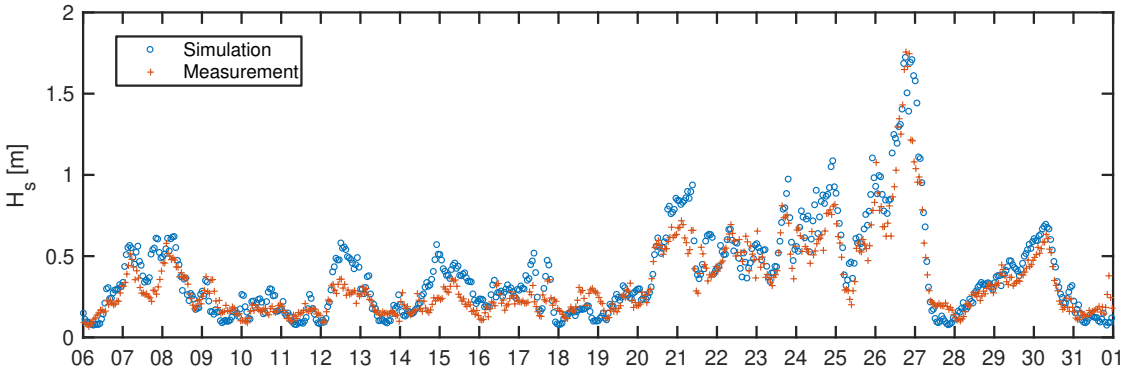

Figure 5: Comparison of measured and simulated significant wave height at DWR3 during a storm event in December 2016.

Fig. 6, exhibit a great scatter, but they all come from the same storm event in December 2016, as shown in Fig. 5.

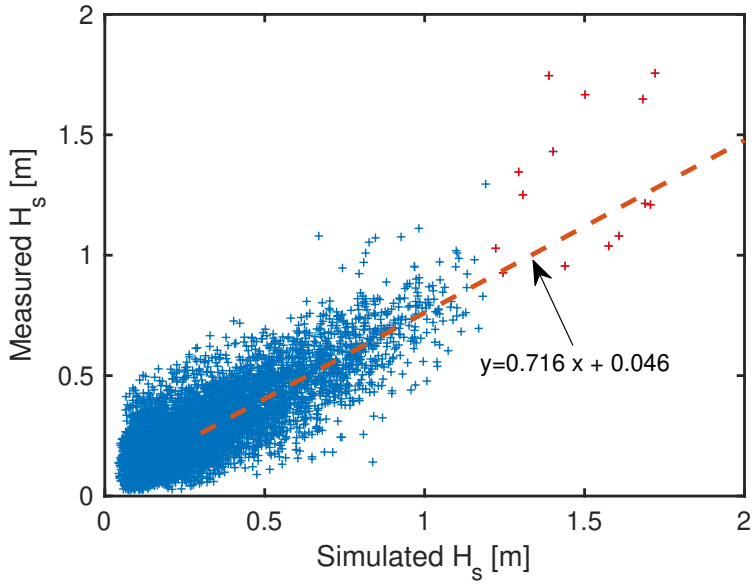

Figure 6: Scatter plot of simulated and measured significant wave height, ΔH_s, from February 2016 to June 2017. Here red + indicates the events with simulated H_s larger than 1.2m. Red dash line denotes the regression line for simulated H_s larger than 0.3m.

This discrepancy is plotted in Fig. 7 and also given in Table A.6 in the appendix. To quantify the discrepancy, root mean square error (RMSE), bias and model uncertainty are introduced here. The RMSE provides a quantitative measure of the model, and the bias indicates the correspondence between the mean values of measured and simulated significant wave height. The RMSE and bias

are defined as follows

$$RMSE = \sqrt{\frac{1}{N}\sum_{j=1}^{N}\left(H_{s,S_j} - H_{s,M_j}\right)^2} \tag{1}$$

$$Bias = \frac{1}{N}\sum_{j=1}^{N}\left(H_{s,S_j} - H_{s,M_j}\right) \tag{2}$$

where N represents the number of measured H_s. The calculated RMSE and bias are 0.105 and 0.007, respectively.

The model uncertainty is defined as the ratio between measured H_s and simulated H_s, given by

$$X = \frac{H_{s,M_j}}{H_{s,S_j}} \tag{3}$$

Model uncertainty for each pair of measured H_s and corresponding simulated H_s can be calculated. However, when the simulated H_s is small, the estimated model uncertainty might be significantly large and is not representative. Therefore, model uncertainty given large simulated H_s is considered here. The mean value and coefficient of variation (CoV) of model uncertainty for simulated H_s larger than 0.6m are 0.767 and 0.228, respectively.

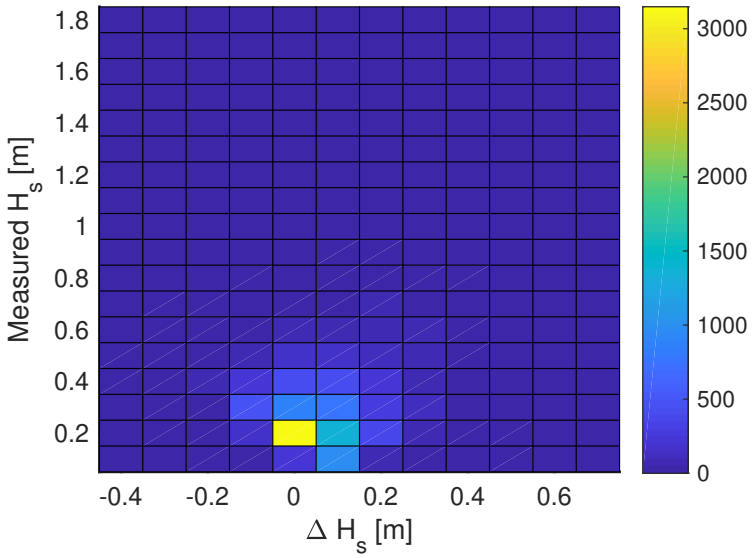

Figure 7: Distribution of the measured significant wave height and the discrepancy between simulated and measured significant wave height from February 2016 to June 2017.

Statistical analysis indicates that 93.2% of total data have a absolute discrepancy $|\Delta H_s|$ less than 0.2m. Moreover, 75.1% of total measured data have a H_s smaller than 0.3m, in which 97.1% are associated with a discrepancy $|\Delta H_s|$ less than 0.2m. This implies that the discrepancies ΔH_s

mainly come from cases with small H_s. One possible reason for these discrepancies is that in the numerical simulations, the cases with small H_s assumes only one dominant direction; however, the measured wave data is usually associated with multiple dominant directions (Cheng et al., 2019b). Another possible reason is due to ship-induced waves captured by the wave buoy. Ship waves might contribute to the discrepancy for small H_s, but for large H_s, the impact of ship waves on the significant wave height is negligible (Cheng et al., 2019b).

3.1. Marginal distribution of significant wave height

The measured and simulated significant wave height at DWR3 from February 2016 to June 2017 are plotted in a Weibull probability paper, as shown in Fig. 8. It can be observed that the upper part of both measured and simulated H_s follow a Weibull distribution. However, the raw data in the lower tail behave differently. Hereinafter, the term raw data means the sample data that is used for fitting of analytical distributions.

For the simulated H_s, raw data with H_s larger than 0.1m follows a Weibull distribution. Since large H_s is significant from design point of view, Weibull model is thus applied for the simulated data. The probability density function (PDF) is given by

$$f_{H_{s,S}}(h) = \frac{\alpha_S}{\beta_S}\left(\frac{h}{\beta_S}\right)^{\alpha_S-1}\exp\left[-\left(\frac{h}{\beta_S}\right)^{\alpha_S}\right] \tag{4}$$

where α_S and β_S denote the shape and scale parameters, respectively.

Regarding the measured H_s, the lower part of the raw data follows a log-normal distribution while the data in the upper tail follow a Weibull distribution. The hybrid lognormal and Weibull distribution, i.e., the Lonowe model developed by Haver (1980) is thus employed to describe the marginal distribution of measured H_s. The PDF is written as

$$f_{H_{s,M}}(h) = \begin{cases} \frac{1}{\sqrt{2\pi}\sigma_M h}\cdot\exp\left[-\frac{1}{2}\left(\frac{\ln(h)-\mu_M}{\sigma_M}\right)^2\right] & \text{if } h \le h_0 \\ \frac{\alpha_M}{\beta_M}\left(\frac{h}{\beta_M}\right)^{\alpha_M-1}\exp\left[-\left(\frac{h}{\beta_M}\right)^{\alpha_M}\right] & \text{if } h > h_0 \end{cases} \tag{5}$$

where h_0 is the shifting point from the lognormal distribution to Weibull distribution, μ_M and σ_M are the mean value and standard deviation of $\ln(H_s)$ in the lognormal distribution. α_M and β_M are the shape and scale parameters in the Weibull distribution. Parameters α_M and β_M are estimated by imposing the continuity condition of PDF and cumulative distribution function (CDF) at the shifting point. Detailed method on estimating the shifting point is described by Haver (1980) and Moan et al. (2005) and is not explained here.

The comparison between the raw data and fitted distribution for both measured and simulated H_s in the Weibull probability paper is demonstrated in Fig. 8. In general, the fitted distribution

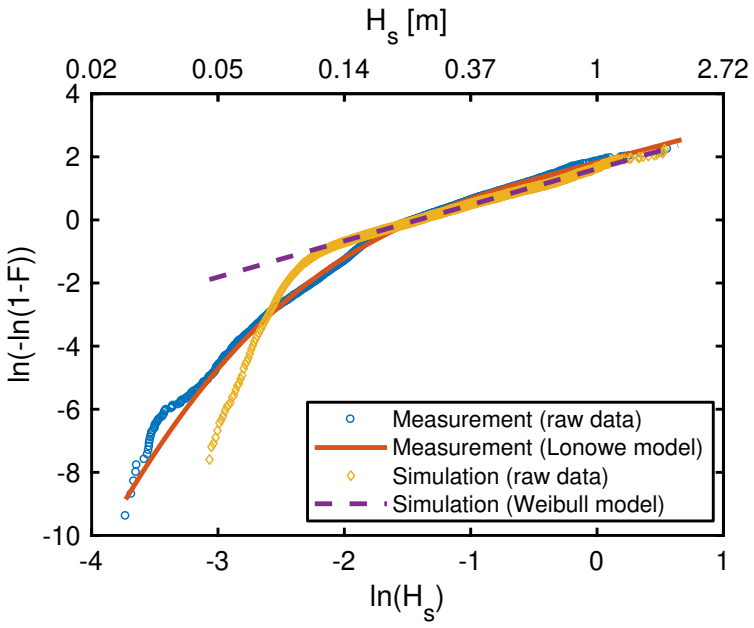

Figure 8: Weibull plot of marginal distribution of simulated and measured significant wave height H_s from February 2016 to June 2017.

and the raw data agree fairly well, except for the lower tail of simulated H_s. The value of Weibull parameters for the simulated and measured H_s is given in Table 1.

Table 1: Comparison of Weibull parameters and significant wave height H_s estimated from measured and simulated wave data based on raw data and fitted distribution. Data from February 2016 to June 2017 is considered here.

Data	Weibull parameters		Raw data	Fitted distribution			
	α	β	1-year Hs	1-year Hs	10-year Hs	50-year Hs	100-year Hs
Measurement	1.071	0.182	1.711	1.425	1.760	1.991	2.090
Simulation	1.145	0.242	1.699	1.664	2.027	2.275	2.381

It can be found that the 1-year H_s estimated from the raw data of measured and simulated H_s is very close, with a difference about 0.7%. It should be noted that the raw data used for estimating the 1-year H_s is from February 2016 to June 2017, about 17 months. Uncertainty might exist in the estimated 1-year H_s from the raw data. The predicted annual extreme value of H_s based on the simulated data is close to that estimated from the raw data. The difference is approximately 2.75%, which is also small. However, the predicted annual extreme value of H_s based on the measured data presents a significant discrepancy, about 16.7%. It underestimates the predicted annual extreme value of H_s. The reason is due to the difference in the fitted parameters, especially the scale parameter, for the Weibull distributions, as given in Table 1. As a result, the predicted 10-year, 50-year and 100-year extreme values of H_s based on the fitted distribution differ significantly between the measured data and simulated data.

3.2. Variation in the wave data

To study the variation of predicted H_s in different years, the fitting procedure described above are applied for measured or simulated data in each year. For the simulated data in 2017, only data in 6 months is used. For the measured data in 2016 and 2018, a duration of about 11 months and 10 months is applied, respectively. The fitting procedure described above is also employed to predict the extreme values of H_s for all measured or simulated data, as shown in Fig. 9.

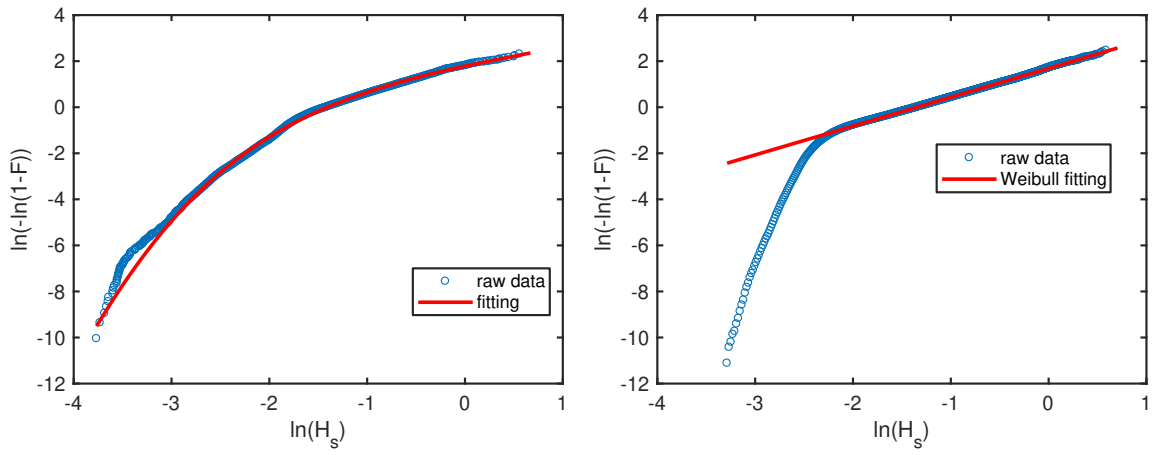

(a) Measured H_s (b) Simulated H_s

Figure 9: Weibull plot of marginal distribution of (a) measured significant wave height H_s based on measured data from 2016 to 2018, (b) simulated significant wave height H_s based on simulated data from 2002 to 2017.

Fig. 10 shows the variations in the mean values of measured and simulated H_s based on annual data, overlap data from February 2016 to June 2017 and all data. The mean values of measured and simulated H_s in each year present certain variation. The mean value and coefficient of variation (CoV) of annual mean H_s for the simulated data is 0.252m and 0.0079, respectively, and for the measured data is 0.241 and 0.0319, respectively. These mean values are very close to the corresponding mean values of annual H_s based on all data, which are 0.252m and 0.241m for the simulated and measured data, respectively. Regarding the overlap data, mean values of measured and simulated H_s are 0.236m and 0.243m, which are fairly close.

Figs. 11 and 12 show the predicted annual and 100-year extreme values of measured H_s by using the Lonowe model and simulated H_s by using the Weibull model, based on annual data, overlap data from February 2016 to June 2017 and all data. These two figures also show the large variations in the predicted extreme values based on the data in different years.

Regarding the simulated data, the annual extreme value varies between a maximum of 1.749m in 2016 and a minimum of 1.227m in 2002, while it is 1.512m based on 16-year simulated data (from 2002 to 2017). The ratio of maximum to minimum of the predicted 100-year extreme value

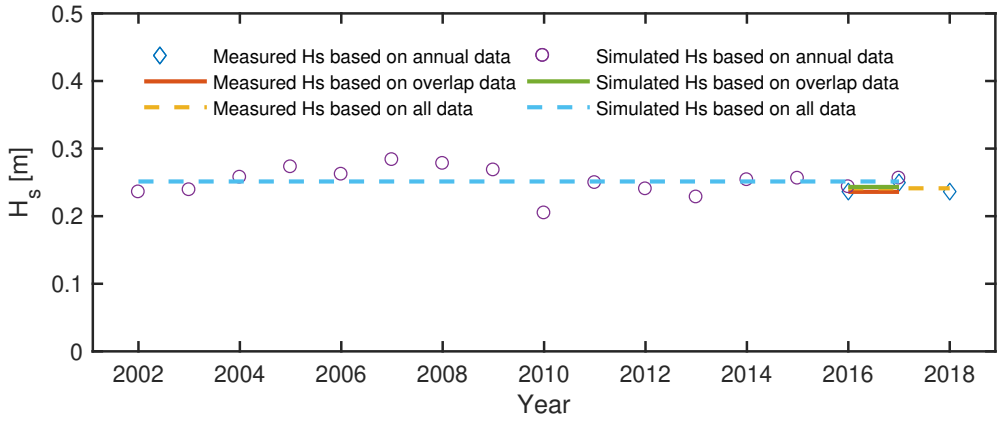

Figure 10: Variations in the mean value of measured and simulated significant wave height estimated based on annual data, overlap data from February 2016 to June 2017 and all data.

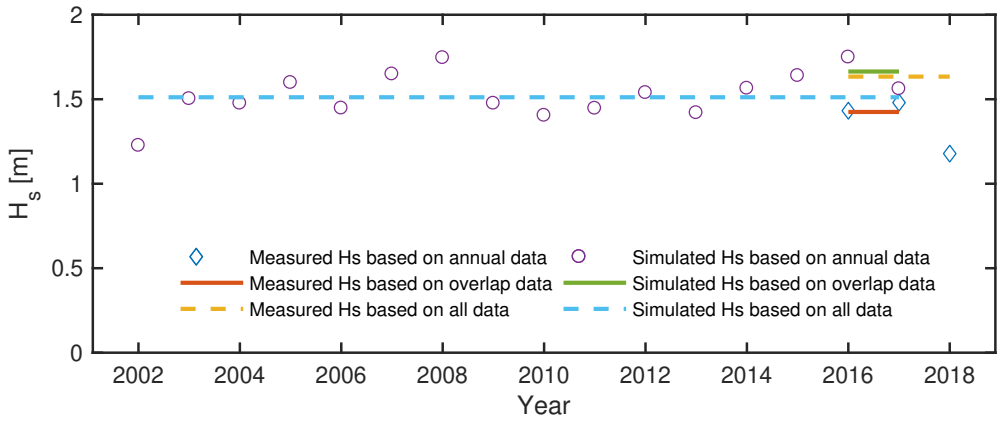

Figure 11: Variations in the annual predicted extreme value of measured and simulated significant wave height estimated based on annual data, overlap data from February 2016 to June 2017 and all data.

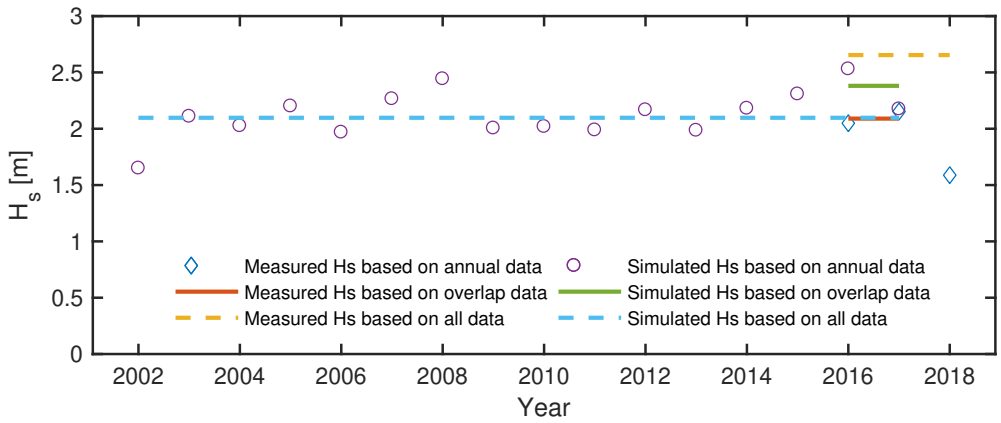

Figure 12: Variations in the predicted 100-year extreme value of measured and simulated significant wave height estimated based on annual data, overlap data from February 2016 to June 2017 and all data.

is about 1.53, varying from 1.650m (corresponding to 2002) to 2.531m (corresponding to 2016). The predicted 100-year extreme value based on 16-year simulated data is about 2.097m. The CoV of predicted annual and 100-year extreme values based on annual simulated data is 0.119 and 0.156, respectively.

The predicted annual extreme values of H_s based on annual measured data in 2016, 2017 and 2018 are 1.432m, 1.480m and 1.178m, respectively. The predicted annual extreme value of H_s based on 3-year (2016-2018) measured data is 1.634m, which is larger than the annual extreme value predicted by annual measured data. The predicted 100-year extreme value of H_s based on 3-year (2016-2018) measured data is 2.654m, which is also much larger than the 100-year extreme values predicted by annual measured data. The differences in predicted 100-year extreme values are due to the fact that very limited data (annual or 3-year measured data) are used to estimate the parameters for the Lonowe model and great uncertainty might exist in the parameter fitting. A larger data basis, e.g. by hincasting, is required to limit the uncertainty in the predicted 100-year extreme value.

4. Prediction of long-term environmental conditions

In this study, the simulated wind and wave data based on the hindcast data are represented in a database for the years 2002-2017. They have been sampled hourly for wind and wave parameters. By assuming sequential stationary short-term conditions, the long-term variation in environmental condition is described by the mean wind speed U_w and wave spectral parameters, significant wave height H_s and peak period T_p. Marginal and joint distribution of wind and wave conditions are approximated by fitting analytical distributions to the raw data. It should be noted that when constructing the joint distributions, the wave data only include wind-generated waves and swell is not considered.

4.1. Marginal distribution of mean wind speed U_w

The mean wind speed considered is at the height of 10m above the sea level. Previous studies, e.g., by Bitner-Gregersen and Haver (1991) and Bitner-Gregersen (2005), have shown that the two-parameter Weibull distribution is a good approximation for modeling wind speed distribution. The PDF is given in Eq. 6.

$$f_{U_w}(u) = \frac{\alpha_U}{\beta_U}\left(\frac{u}{\beta_U}\right)^{\alpha_U-1}\exp\left[-\left(\frac{u}{\beta_U}\right)^{\alpha_U}\right] \tag{6}$$

where α_U and β_U denote the shape and scale parameters, respectively, and u is mean wind speed variable. Fig. 13 shows the fitted marginal distribution curve of the 1-hour mean wind speed at

10m height on the Weibull probability paper. A good agreement between the raw data and the fitted curve is observed.

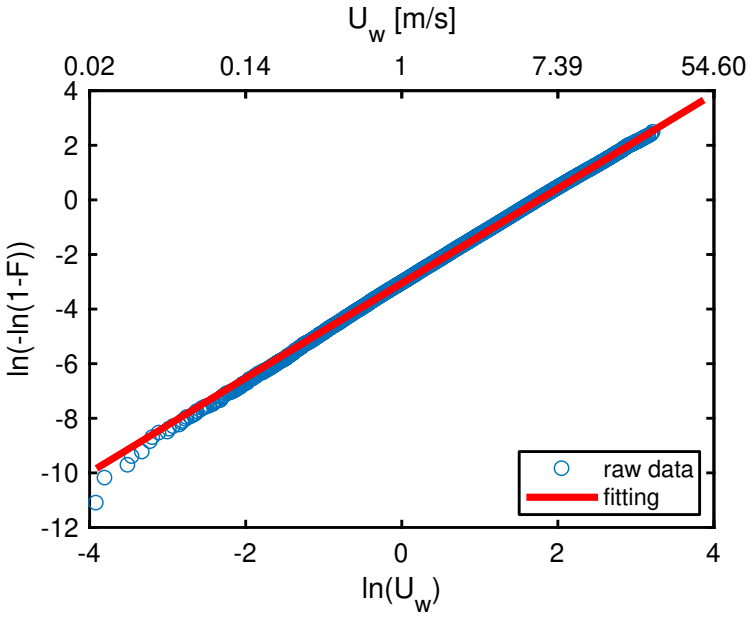

Figure 13: Weibull plot of marginal distribution of mean wind speed U_w.

4.2. Joint distribution of H_s and T_p

If only wave data is considered, the joint distribution of H_s and T_p consists of a marginal distribution of H_s and a conditional distribution of T_p given H_s

$$f_{H_s,T_p}(h,t) = f_{H_s}(h) f_{T_p|H_s}(t|h) \tag{7}$$

where h and t are significant wave height and peak period variables, respectively. $f_{H_s}(h)$ is the marginal distribution of H_s, which is given by Eq. 4 and shown in Fig. 9(b) for the simulated wave data. $f_{T_p|H_s}(t|h)$ is the conditional PDF of T_p given H_s.

According to previous studies (Bitner-Gregersen, 2012; Johannessen et al., 2002; Li et al., 2015), the conditional distribution of T_p given H_s seems to follow a lognormal distribution

$$f_{T_p|H_s}(t|u,h) = \frac{1}{\sqrt{2\pi}\sigma_{LT} t} \cdot \exp\left[-\frac{1}{2}\left(\frac{\ln(t)-\mu_{LT}}{\sigma_{LT}}\right)^2\right] \tag{8}$$

where μ_{LT} and σ_{LT} are the mean value and standard deviation of $\ln(t)$.

The peak period data is resampled into different H_s classes with a bin size of 0.1m, and is then plotted in a lognormal probability paper. Fig. 14 shows the fitted lognormal distribution curves

of T_p at a low H_s class and at a high H_s class. It can be found that the lognormal distribution is reasonable for both low and high H_s classes. For each H_s class, μ_{LT} and σ^2_{LT} can be estimated. They are thus expressed as a function of H_s in order to describe the conditionality of T_p on H_s.

$$\mu_{LT} = e_1 \cdot h^{e_2} + e_3 \tag{9}$$

$$\sigma^2_{LT} = k_1 \cdot h^{k_2} + k_3 \tag{10}$$

in which e_1, e_2, e_3, k_1, k_2, and k_3 are the parameters estimated from the raw data by nonlinear curve fitting. The curve fitting results are shown in Fig. 15.

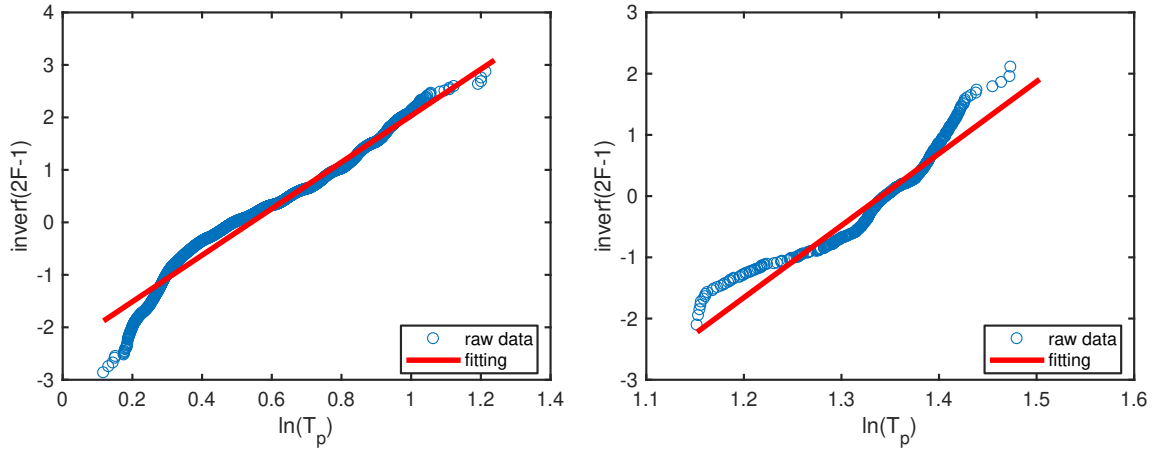

(a) 0.2m < H_s < 0.3m (b) 1.0m < H_s < 1.1m

Figure 14: Lognormal plot of conditional distribution of T_p given H_s.

As a summary, the parameters in the joint distribution of H_s and T_p are estimated by fitting raw data into analytical distribution, and are given in Tables 2.

Table 2: Parameters for the marginal distribution of H_s, $f_{H_s}(h)$, the conditional distribution of T_p given H_s, $f_{T_p|H_s}(t|h)$.

Distributions	Parameter	Associated equation	DWR3
Marginal H_s	α_S	Eq. 4	1.256
	β_S	Eq. 4	0.261
Conditional T_p given H_s	e_1	Eq. 9	-6.727
	e_2	Eq. 9	-0.060
	e_3	Eq. 9	8.088
	k_1	Eq. 10	0.002
	k_2	Eq. 10	-1.397
	k_3	Eq. 10	0.002

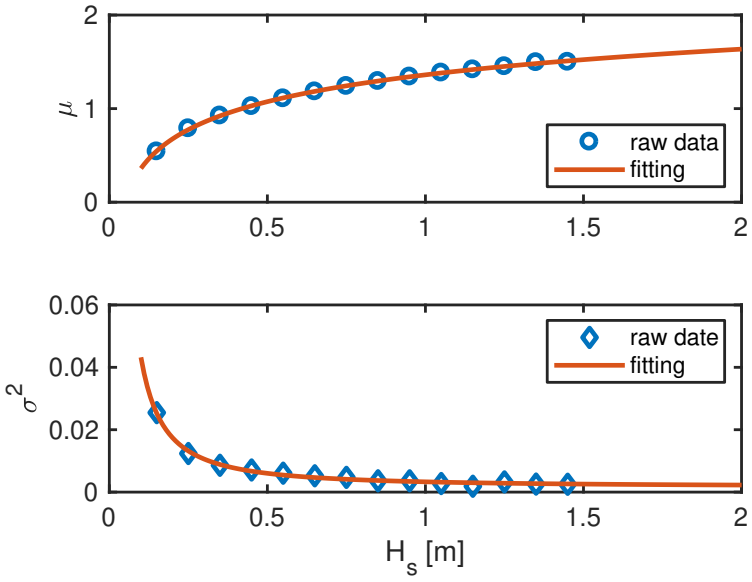

Figure 15: Nonlinear fitting of lognormal parameters for conditional distribution of T_p given H_s.

4.3. Joint Distribution of U_w, H_s and T_p

The joint distribution of U_w, H_s and T_p is expressed as follows

$$f_{U_w,H_s,T_p}(u,h,t) = f_{U_w}(u) f_{H_s|U_w}(h|u) f_{T_p|U_w,H_s}(t|u,h) \tag{11}$$

in which $f_{U_w}(u)$ is a marginal distribution of U_w as given by Eq. 6, $f_{H_s|U_w}(h|u)$ is a conditional distribution of H_s given U_w, and $f_{T_p|U_w,H_s}(t|u,h)$ is a conditional distribution of T_p given both U_w and H_s. In this section, the estimations of $f_{H_s|U_w}(h|u)$ and $f_{T_p|U_w,H_s}(t|u,h)$ are explained in detail. The development of joint distribution in terms of conditional distributions has been used by Johannessen et al. (2002), Li et al. (2015) and Horn et al. (2018). In this paper the procedure used follows the work by Li et al. (2015) and Johannessen et al. (2002).

4.3.1. Conditional distribution of H_s given U_w

Considering a bin size of 1m/s for the mean wind speed U_w, the significant wave height H_s is resampled according to U_w classes. To fit the conditional PDF of H_s given U_w, the raw data in each wind speed class is plotted in the Weibull probability paper. Fig. 16 shows two examples of raw data at two different U_w classes. It appears that the raw data in the medium and high wind speed classes follow the Weibull model for the conditional distribution of H_s. However, in the low wind speed classes, the Weibull model is only suitable for H_s larger than 0.1m. To improve the accuracy of fitted distribution for H_s at high wind speed classes, the Weibull model is considered for all wind speed classes.

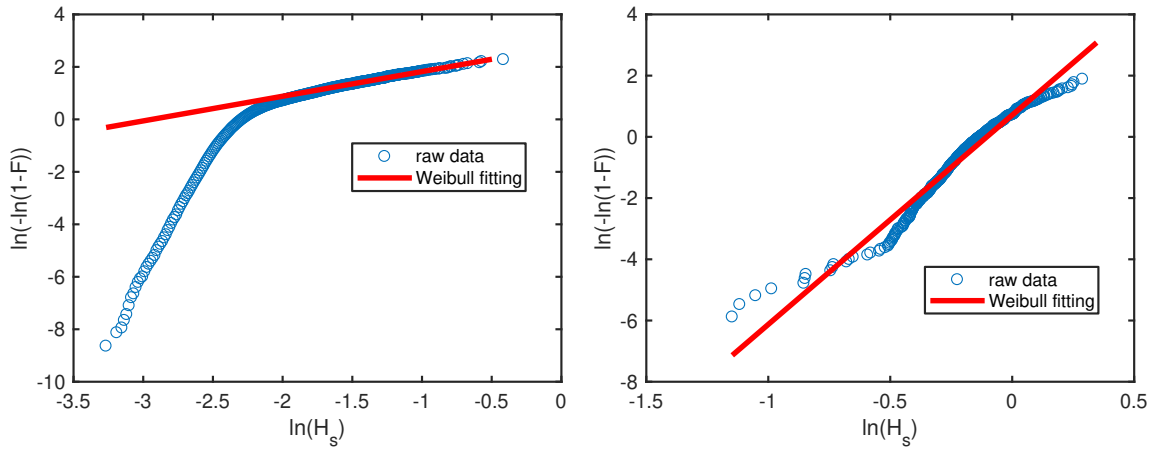

(a) 2m/s < U_w < 3m/s (b) 14m/s < U_w < 15m/s

Figure 16: Weibull plot of conditional distribution of H_s given U_w.

Therefore, the conditional PDF of H_s given U_w is described by a two-parameter Weibull distribution, as follows

$$f_{H_s|U_w}(h|u) = \frac{\alpha_{HC}}{\beta_{HC}}\left(\frac{h}{\beta_{HC}}\right)^{\alpha_{HC}-1}\exp\left[-\left(\frac{h}{\beta_{HC}}\right)^{\alpha_{HC}}\right] \tag{12}$$

where α_{HC} and β_{HC} denote the shape and scale parameters, respectively. For each wind speed class, a pair of shape and scale parameters is achieved. The shape and scale parameters are then fitted as power functions of mean wind speed to represent the conditionality.

$$\alpha_{HC} = a_1 \cdot u^{a_2} + a_3 \tag{13}$$

$$\beta_{HC} = b_1 \cdot u^{b_2} + b_3 \tag{14}$$

in which a_1, a_2, a_3, b_1, b_2, and b_3 are the parameters estimated from the raw data by nonlinear curve fitting. The curve fitting results are shown in Fig. 17.

4.3.2. Conditional distribution of T_p given U_w and H_s

The peak period data is resampled in different wind-wave classes by considering a bin size of 1m/s for the mean wind speed U_w and a bin size of 0.1m for the significant wave height H_s. The data in each wind-wave class indicate a lognormal distribution for the conditional distribution of

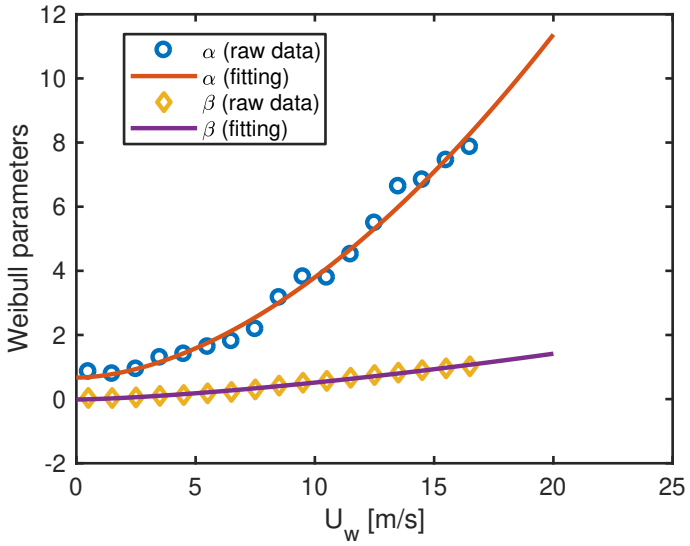

Figure 17: Nonlinear fitting of Weibull parameters for conditional distribution of H_s given U_w.

T_p given U_w and H_s, whose PDF is given by

$$f_{T_p|U_w,H_s}(t|u,h) = \frac{1}{\sqrt{2\pi}\sigma_{\ln(T_p)}t} \cdot \exp\left[-\frac{1}{2}\left(\frac{\ln(t)-\mu_{\ln(T_p)}}{\sigma_{\ln(T_p)}}\right)^2\right] \tag{15}$$

where $\mu_{\ln(T_p)}$ and $\sigma_{\ln(T_p)}$ are the parameters in the conditional lognormal distribution, i.e., the mean value and standard deviation of $\ln(t)$ at each combination of wind-wave class. The parameters $\mu_{\ln(T_p)}$ and $\sigma_{\ln(T_p)}$ are functions of both U_w and H_s and can be estimated by using the following relationships

$$\mu_{\ln(T_p)} = \ln\left(\frac{\mu_{T_p}}{\sqrt{1+\upsilon_{T_p}^2}}\right) \tag{16}$$

$$\sigma_{\ln(T_p)}^2 = \ln\left(1+\upsilon_{T_p}^2\right) \tag{17}$$

$$\upsilon_{T_p} = \frac{\sigma_{T_p}}{\mu_{T_p}} \tag{18}$$

where μ_{T_p} and σ_{T_p} are the mean value and standard deviation of T_p in each wind-wave class, respectively. υ_{T_p} is the coefficient of variation (CoV) of T_p.

To express the conditionality, we need to fit μ_{T_p} and υ_{T_p} as functions of U_w and H_s. Fig. 18 shows the variations of μ_{T_p} and υ_{T_p} in terms of U_w and H_s. It should be noted that the wind-wave classes with limited data are excluded to avoid large uncertainties.

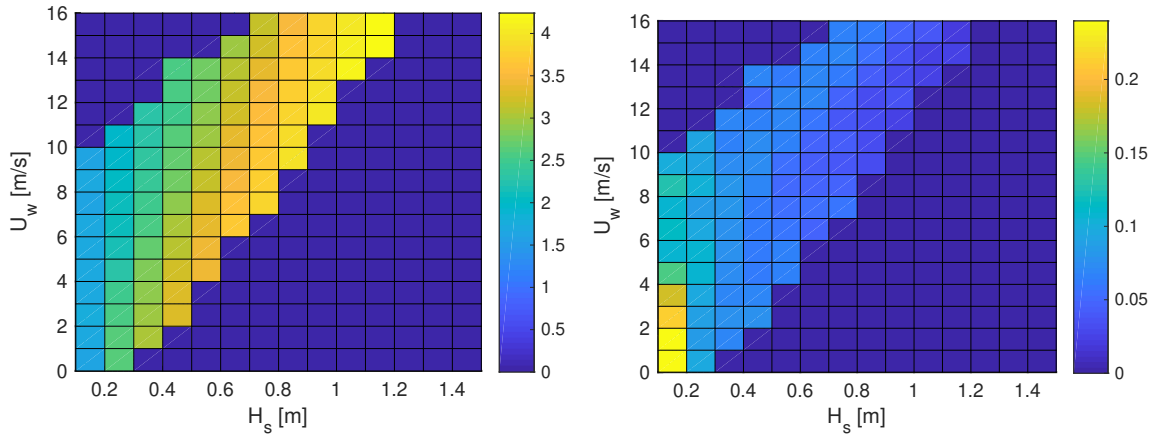

(a) Mean value of T_p, μ_{T_p} (b) CoV of T_p, υ_{T_p}

Figure 18: Mean value and coefficient of variation (CoV) of T_p for each wind-wave class.

It can be observed that μ_{T_p} and υ_{T_p} are primarily dependent on H_s and they shift with the variation of wind speed. The method proposed by Johannessen et al. (2002) is employed in this study to estimate the parameters of T_p in the lognormal distribution. The mean value of T_p is modeled by using the following equation:

$$\mu_{T_p} = \bar{t}(u,h) = \bar{t}(h) \cdot \left[1 + \vartheta \left(\frac{u - \bar{u}(h)}{\bar{u}(h)}\right)^{\gamma}\right] \tag{19}$$

where ϑ and γ are fitting coefficients; $\bar{t}(h)$ and $\bar{u}(h)$ are the expected peak period and mean wind speed for a given value of H_s. Here, $\bar{t}(h)$ and $\bar{u}(h)$ are fitted as a function of H_s

$$\bar{t}(h) = c_1 \cdot h^{c_2} + c_3 \tag{20}$$

$$\bar{u}(h) = d_1 \cdot h^{d_2} + d_3 \tag{21}$$

in which c_1, c_2, c_3, d_1, d_2, and d_3 are the parameters estimated from the raw data by nonlinear curve fitting.

The term $\left[1 + \vartheta \left(\frac{u-\bar{u}(h)}{\bar{u}(h)}\right)^{\gamma}\right]$ in Eq. 19 adjusts the expected T_p according to whether the actual wind speed is above or below the expected wind speed for the particular significant wave height. To estimate parameters ϑ and γ, Eq. 19 can be rewritten as

$$\frac{\bar{t}(u,h) - \bar{t}(h)}{\bar{t}(h)} = \vartheta \left(\frac{u - \bar{u}(h)}{\bar{u}(h)}\right)^{\gamma} \tag{22}$$

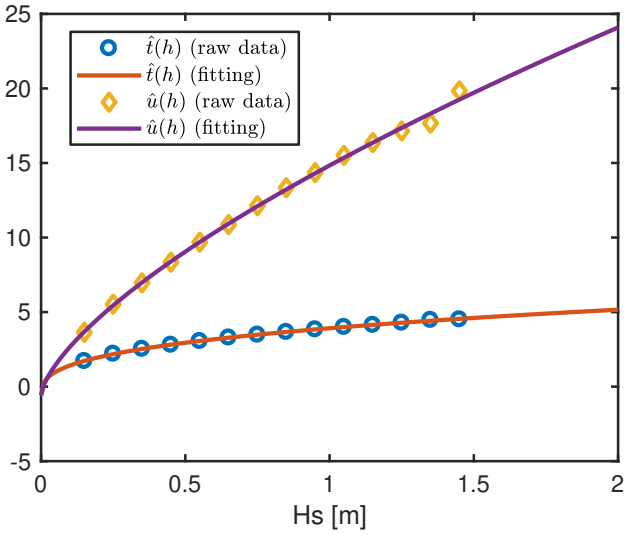

Figure 19: Nonlinear fitting of expected peak period $\bar{t}(h)$ and mean wind speed $\bar{u}(h)$ for conditional distribution of T_p given U_w and H_s.

where $\frac{\bar{t}(u,h)-\bar{t}(h)}{\bar{t}(h)}$ and $\frac{u-\bar{u}(h)}{\bar{u}(h)}$ are normalized peak period and wind speed, respectively. For each H_s class, the normalized peak period is plotted as a function of the normalized wind speed. Nearly
345 linear relationships are observed for most H_s classes, indicating that γ is close to 1. Moreover, ϑ estimated for each H_s class is shown in Fig. 20, A mean value of ϑ for high H_s classes (larger than 0.2m) is thus adopted and used in Eq. 22.

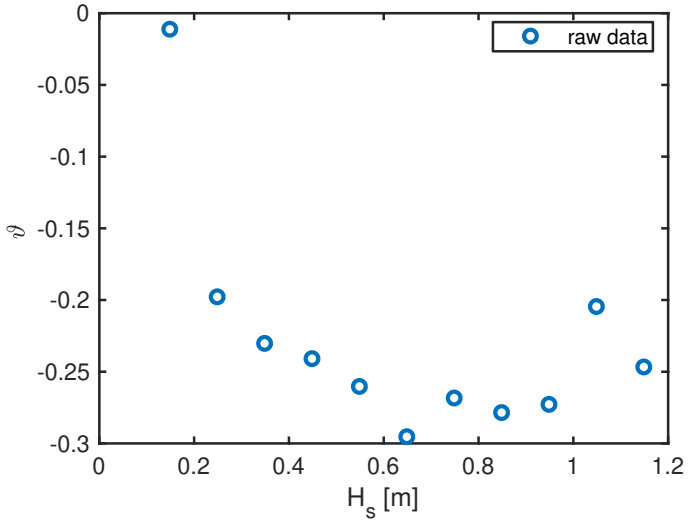

Figure 20: Nonlinear fitting of parameter ϑ for conditional distribution of T_p given U_w and H_s.

In addition, the coefficient of variation can be assumed to be a function of only H_s

$$\upsilon_{T_p}(h) = f_1 \cdot h^{f_2} + f_3 \tag{23}$$

where f_1, f_2, and f_3 are the parameters from nonlinear curve fitting, as shown in Fig. 21.

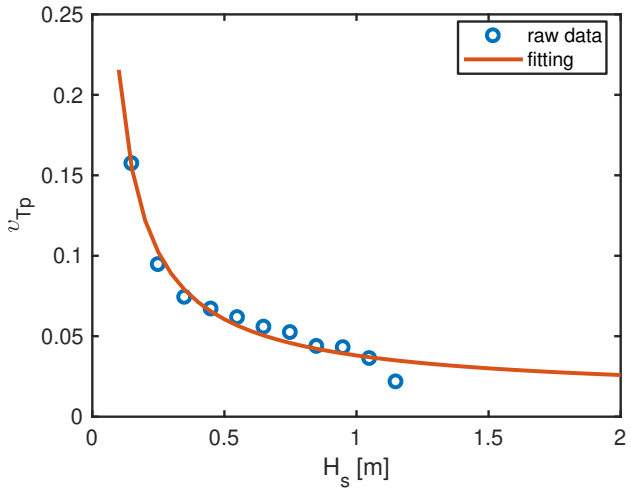

Figure 21: Nonlinear fitting of parameter υ_{T_p} for conditional distribution of T_p given U_w and H_s.

By fitting the raw data with analytical distributions, the parameters in the long-term joint distribution of U_w, H_s and T_p can be estimated, as given in Table 3.

4.4. Environmental contour surface

Based on the joint distribution, a environmental contour corresponding to a given return period can be achieved. The environmental contour provides a simplified approach to predict the long-term extreme response. To construct the environmental contour, the physical variables in the joint distribution are usually transferred into a nonphysical space (i.e., U space) consisting of several independent standard and normal variables. Such a transformation is generally carried out by using the Rosenblatt transformation (Madsen et al., 2006).

For the joint distribution of U_w, H_s and T_p given by Eq. 11, the following three variables in the U space are introduced

$$\begin{aligned} U_1 &= \Phi^{-1}(F_{U_w}(u)) \\ U_2 &= \Phi^{-1}(F_{H_s|U_w}(h|u) \\ U_3 &= \Phi^{-1}(F_{T_p|U_w,H_s}(t|u,h) \end{aligned} \tag{24}$$

where $\Phi()$ is the CDF of standard normal distribution, and F represents the CDF of the original random variables. Therefore, these three variables in the U space represent the marginal distribution of U_w, the conditional distribution of H_s given U_w, and the conditional distribution of T_p

Table 3: Parameters for the marginal distribution of U_w, $f_{U_w}(u)$, the conditional distribution of H_s given U_w, $f_{H_s|U_w}(h|u)$, and the conditional distribution of T_p given both U_w and H_s, $f_{T_p|U_w,H_s}(t|u,h)$.

Distributions	Parameter	Associated equation	DWR3
Marginal U_w	α_U	Eq. 6	1.735
	β_U	Eq. 6	5.805
Conditional H_s given U_w	a_1	Eq. 13	0.053
	a_2	Eq. 13	1.774
	a_3	Eq. 13	0.671
	b_1	Eq. 14	0.019
	b_2	Eq. 14	1.436
	b_3	Eq. 14	-0.012
Conditional T_p given U_w and H_s	c_1	Eq. 20	4.509
	c_2	Eq. 20	0.351
	c_3	Eq. 20	-0.592
	d_1	Eq. 21	15.388
	d_2	Eq. 21	0.679
	d_3	Eq. 21	-0.556
	ϑ	Eq. 19	-0.25
	γ	Eq. 19	1.0
	f_1	Eq. 23	0.026
	f_2	Eq. 23	-0.887
	f_3	Eq. 23	0.012

given U_w and H_s, respectively. They are then used to construct a 3-dimensional sphere in the U space, with a radius, r, given by

$$\Phi(r) = 1 - P_f = 1 - \frac{1}{N_y} \tag{25}$$

where $P_f = 1/N_y$ is the failure probability corresponding to the N-year return period, and N_y is the total number of 1-hour sea state in N years. By transforming the variables in the U space into the physical space, we can obtain the environmental contour surface.

The three-dimensional 100-year environmental contour surface of U_w, H_s and T_p is demonstrated in Fig. 22. Contour lines of H_s and T_p at several different levels of U_w are also shown in Fig. 22. From the 100-year environmental contour surface, two particular extreme conditions, i.e., one with maximum mean wind speed U_w and the other with maximum significant wave height, are identified, as given in Table 4. These two extreme conditions have fairly close values in terms of mean wind speed, significant wave height and peak period. In other words, the maximum mean wind speed is highly correlated to the maximum significant wave height. This is because the waves are mainly generated by local winds and the sea condition is considered as fetch limited. According to Carter (1982) and Tucker and Pitt (2001), the significant wave height and peak period for

fetch-limited seas in deep water is given by,

$$H_s = 0.0163\sqrt{L_f}U_w \tag{26}$$

$$T_p = 0.566{L_f}^{0.3}U_w^{0.4} \tag{27}$$

where L_f is the fetch length in km. The topography shown in Fig. 1 indicates the fetch length is limited. The longest fetch length in northwest and east directions are about 20km and 23km, respectively. Therefore, the fetch length calculated from Eq. 26 under these two extreme conditions agrees well with the values measured from Fig. 1.

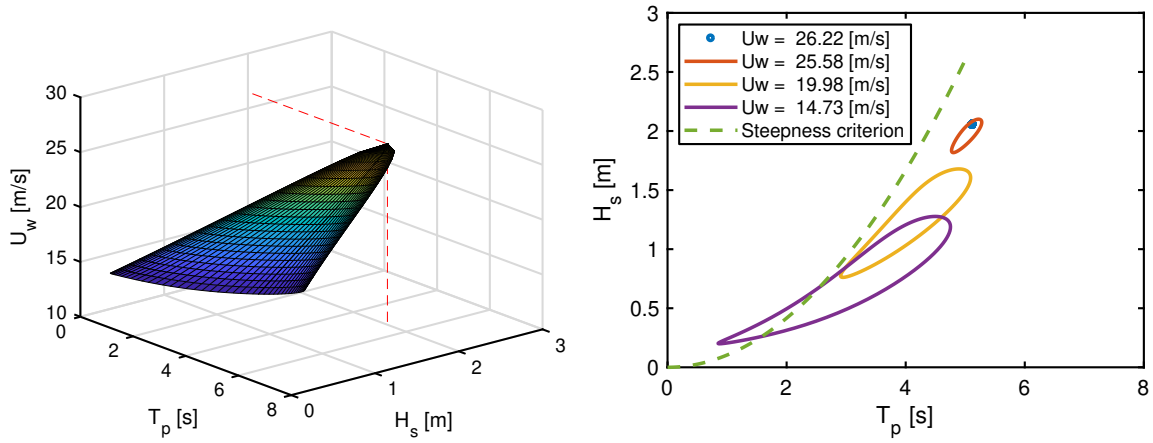

(a) Contour surface

(b) H_s and T_p Contour lines

Figure 22: (a)100-year contour surface of U_w, H_s, and T_p. The red dash lines indicate the projection of the condition with maximum U_w. (b) 100-year contour lines of H_s and T_p under different levels of U_w. The wave steepness criterion is also plotted by the green dash line. According to DNV GL (2014), the limiting value of average wave steepness is $S_p = \frac{2\pi}{g}\frac{H_s}{T_p^2} = \frac{1}{15}$ for $T_p \leq 8$s.

Table 4: Environmental conditions on the 100-year and 10000-year contour surface with the maximum U_w or maximum H_s

Return period	Condition	U_w [m/s]	H_s [m]	T_p [s]
100 year	Condition with maximum U_w	26.22	2.05	5.12
	Condition with maximum H_s	25.87	2.11	5.22
10000 year	Condition with maximum U_w	31	2.63	5.65
	Condition with maximum H_s	30.21	2.66	5.73

The average wave steepness for a short-term sea state is defined as $S_p = \frac{2\pi}{g}\frac{H_s}{T_p^2}$. According to DNV GL (2014), the limiting values of S_p for peak period $T_p \leq 8$s is about $S_p = 1/15$ based on measured data from the Norwegian Continental Shelf. This wave steepness criterion is also

plotted in Fig. 22(b). Under a low mean wind speed, the 100-year contour lines of H_s and T_p might slightly exceed the steepness criterion for sea states with small sea states. Two possible reasons are envisaged for this: one is due to parameter uncertainties in the fitting of raw data by analytical distributions for small sea states, especially in the estimation of conditional distribution of T_p given U_w and H_s; the other one is that the limiting value of wave steepness is developed mainly for open seas and might not be suitable for the fjord considered since the wind-generated waves in the fjord considered are strongly affected by limited fetch length and limited duration especially for small sea states.

Fig. 23 shows the three-dimensional 10000-year environmental contour surface of U_w, H_s and T_p and the contour lines of H_s and T_p at several different levels of U_w. The wave steepness criterion is also plotted in the figure. In general, the 10000-year contour surface and contour lines exhibit similar trends as the 100-year contour surface and contour lines.

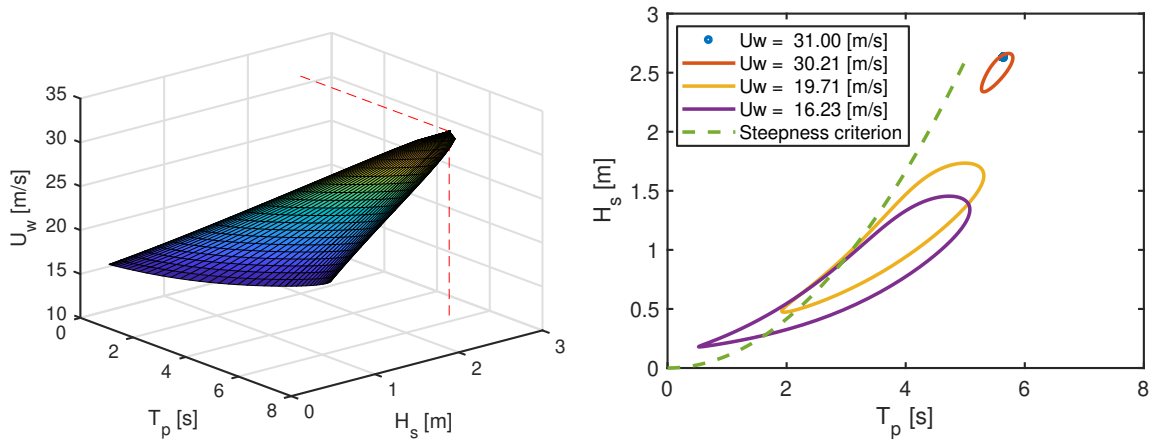

(a) Contour surface

(b) H_s and T_p Contour lines

Figure 23: (a)10000-year contour surface of U_w, H_s, and T_p. The red dash lines indicate the projection of the condition with maximum U_w. (b) 10000-year contour lines of H_s and T_p under different levels of U_w. The wave steepness criterion is also plotted by the green dash line.

5. Discussions

5.1. Uncertainty in the joint distribution

Uncertainties exist in the joint distribution. The main sources of uncertainties are related to the accuracy of simulated wind and wave data, the amount of data and the model used in this study.

The joint distribution is constructed by using simulated wind and wave data based on hindcast environmental data. An indication of the accuracy of simulated wave data is obtained in this study by comparison against field measurements. An overall good agreement is observed with respect to

significant wave height. However, the accuracy of simulated wind data is not studied and validated yet. It can introduce an uncertainty in the joint distribution.

The joint distribution consists of a marginal distribution and conditional distributions. It should be established by using sufficient long-term wind and wave data in order to reduce the statistical uncertainty. In this study, about 16-years of simulated wind and wave data are used. It is thus inevitable that statistical uncertainty exists, in particular in the fitting of conditional distribution, because of limited data. This fact can be observed in Section 4. The marginal distribution of mean wind speed can be well fitted by the two-parameter Weibull distribution, as shown in Fig. 13. However, due to lack of data in certain wind and wave conditions, fitting of conditional distribution of H_s given U_w is not accurate for some wind classes, as shown in Fig. 16. Some wind and wave classes have to be excluded when estimating the conditional distribution of H_s given U_w and T_p, as shown in Fig. 18. In addition, the choice of bin size of the environmental parameters affects the number of samples in conditional distribution, which may cause statistical uncertainty.

Model uncertainty is introduced through the choice of probability distribution types to describe the marginal and conditional distribution. The two-parameter Weibull distribution is applied to describe the marginal distribution of simulated H_s. However, as shown in Fig. 9, a large discrepancy is observed in the low tail, i.e., for $H_s < 0.1$m, between the raw data and the analytical Weibull distribution model. A more suitable analytical distribution model that gives good agreement in both upper and low tails is not available. Since extreme environmental conditions are of interest in this study, distribution fitting is thus conducted by concentrating on the upper tail, instead of the whole raw data. Large discrepancies are also observed between the raw data and analytical distribution model when fitting the conditional distributions of H_s given U_w and T_p given U_w and H_s. The focus is on the upper tail region in the raw data to ensure the accuracy of extreme environmental conditions.

5.2. Simplified joint distribution of U_w, H_s, and T_p

Li et al. (2015) proposed a simplified joint distribution of U_w, H_s, and T_p, in which the conditional distribution of T_p given both U_w and H_s is simplified by the conditional distribution of T_p given only H_s. The simplified joint distribution of U_w, H_s and T_p is written as

$$f_{U_w,H_s,T_p}(u,h,t) = f_{U_w}(u) f_{H_s|U_w}(h|u) f_{T_p|H_s}(t|h) \tag{28}$$

Such a simplification is reasonable and also applicable for the present study. The determination of conditional distribution of T_p on U_w and H_s following the method described by Johannessen et al. (2002) is very complicated and may cause large statistical uncertainty due to limited data for conditional probabilities. Moreover, the raw data shown in Fig. 18 indicates that the distribution

of T_p is mainly dependent on H_s, while its dependency on U_w is limited.

Following the simplified method, 100-year environmental contour surface can be obtained, as shown in Fig. 24. Contour lines of H_s and T_p at several different levels of U_w are also demonstrated in Fig. 24. By comparing the contour surface derived from the simplified joint PDF (Eq. 28) with that from the complete joint PDF (Eq. 11), it can be found that

- The critical environmental conditions on the 100-year contour surfaces with maximum U_w or maximum H_s are almost identical by applying the complete and simplified joint PDF. The difference with respect to environmental parameters is smaller than 1.5%.
- For a given U_w level, the T_p value at critical conditions that corresponds to the largest H_s is also very close by using the complete and simplified joint PDF. The discrepancy decreases with the increase of U_w.
- By applying the complete joint PDF, the shape of contour lines of H_s and T_p for a given U_w level is skewed towards small T_p for small H_s. This is also observed by Li et al. (2015), due to the consideration of dependency of T_p on U_w. Local wind can increase the steepness of wave, causing a smaller T_p at the same H_s level.

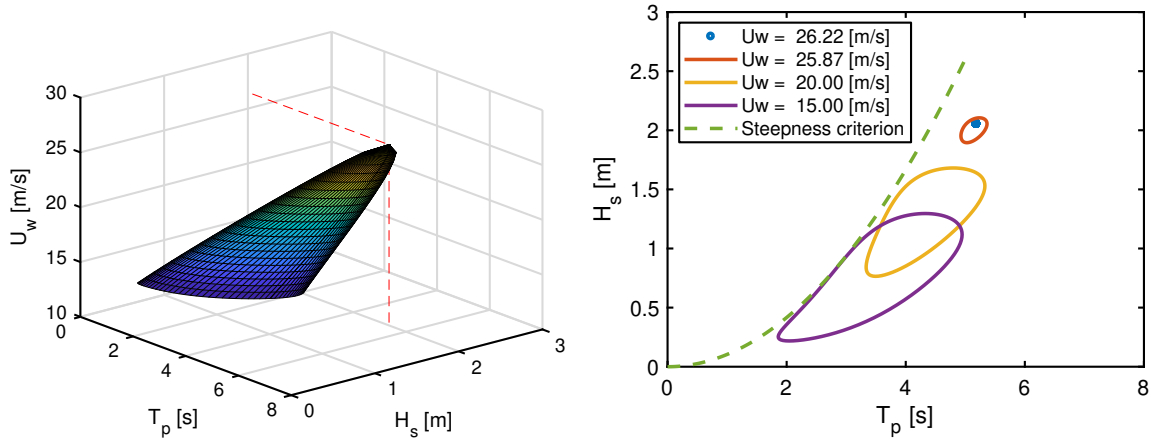

(a) Contour surface

(b) H_s and T_p Contour lines

Figure 24: (a)100-year contour surface of U_w, H_s, and T_p based on simplified joint distribution. The red dash lines indicate the projection of the condition with maximum U_w. (b) 100-year contour lines of H_s and T_p under different levels of U_w based on the simplified joint distribution. The wave steepness criterion is also plotted by the green dash line. According to DNV GL (2014), the limiting value of average wave steepness is $S_p = \frac{2\pi}{g}\frac{H_s}{T_p^2} = \frac{1}{15}$ for $T_p \leq 8$s.

Therefore, the simplified joint distribution of U_w, H_s, and T_p does not affect the determination of critical environmental conditions for design. Based on studies by Cheng et al. (2019a, 2018), dynamic response of a typical extra-long floating bridge is strongly affected by resonant responses,

and these dominant response modes have a natural period larger than 7s. That means that the extra-long floating bridge considered by Cheng et al. (2019a, 2018) is not sensitive to small Tp. For design of such extra-long floating bridges, the simplified joint distribution can thus be an alternative method to construct the environmental contour surface. However, if the structure is sensitive to small T_p, the complete joint distribution should be used.

5.3. Joint environmental models in a fjord versus open seas

As discussed in the introduction, the long-term joint environmental model in a fjord or strait differs from that in the open seas, because the waves in a fjord are mainly wind-generated and are strongly affected by the duration and fetch length. This can be further illustrated by comparing the joint PDF and contour surfaces of U_w, H_s, and T_p presented in this study for a fjord with those given by Li et al. (2015) for open seas. It can be found that

- The joint PDF in a fjord is dominated by environmental conditions with small H_s and T_p, because they are mainly wind-generated and fetch-limited. However, the joint PDF for open seas covers a much broader range of H_s and T_p for the dominant environmental conditions.
- The maximum U_w along the contour surface for a fjord is likely to correspond to the maximum H_s, as given in Table 4. However, regarding the contour surface for open seas, the extreme environmental conditions with maximum H_s and with maximum U_w differs significantly, as described by Li et al. (2015).

As a matter of the fact, high correlations exist in the environmental parameters in a fjord. Table 5 gives the correlation matrix between U_w, H_s, and T_p based on simulated data over about 16 years. The correlation coefficients between U_w and H_s and between H_s and T_p are both very high, larger than 0.91. Moreover, since the maximum U_w and maximum H_s occur almost concurrently for the joint PDF in a fjord, the corresponding sea state is thus likely to cause the largest short-term extreme response and can be considered as the most critical sea state. This also implies that the joint PDF in a fjord can consider much fewer sea states in order to identify the most critical sea state, compared to the joint PDF for open seas. In general, the 'actual critical sea state' should be further verified by considering several sea states around the estimated critical sea state.

Table 5: Correlation matrix of U_w, H_s, and T_p based on simulated data from 2002 to 2017.

	U_w	H_s	T_p
U_w	1	0.915	0.802
H_s	0.915	1	0.924
T_p	0.802	0.924	1

5.4. Application for design of floating bridges

The developed joint PDF or N-year environmental contour surface of U_w, H_s, and T_p can be used to predict the long-term extreme responses for ULS design check of floating bridges, based on the environmental contour method. The sea state with the maximum U_w or maximum H_s can be considered as the most critical short-term sea state. The viability of short-term extreme response is considered by multiplying a correction factor (1.1-1.3) or by using a higher quantile (75-90%) for the short-term extreme response. The value of correction factor or quantile should be calibrated by comparison with a full long-term analysis. This calibration process for a cable-supported bridge with floating pylons is demonstrated by Xu et al. (2018).

6. Conclusions

Long-term joint distribution of parameters for environmental conditions in a Norwegian fjord is addressed in this study for design of floating bridges based on numerically simulated wind and wave data from 2002 to 2017. The joint distribution is expressed as analytical functions in terms of mean wind speed U_w, significant wave height H_s and peak period T_p, by assuming sequential stationary short-term conditions, each with a duration of one hour.

The wind and wave data are numerically generated by using the WRF model and SWAN model, respectively. The accuracy of simulated wave data is validated by comparison against field measurements during the period from February 2016 to June 2017. The time series of simulated H_s has an overall good agreement with the measured H_s. The marginal distributions of measured and simulated H_s are similar for large H_s, but differ for small H_s. Uncertainty in the predicted annual and 100-year extreme values of H_s is also addressed by considering yearly and all data. Since measured data is limited, simulated data need to be used for analyzing the long-term joint distribution.

The parameters for the joint distribution are estimated by fitting the hourly sampled data with analytical distributions. The marginal distribution of U_w, joint distribution of H_s and T_p, and joint distribution of U_w, H_s, and T_p are all presented. Based on the joint distribution, the 100-year contour surface of wind and wave parameters are established. The design points, i.e., environmental conditions with maximum U_w and with maximum H_s, on the 100-year contour surface are also suggested for long-term extreme response analysis by using the environmental contour method.

Compared to the joint distribution of U_w, H_s, and T_p for open seas, the joint distribution in a fjord is dominated by environmental conditions with small H_s and T_p, because they are mainly wind-generated under limited fetch. The extreme environmental condition with maximum U_w and with maximum H_s are fairly close for the joint distribution in a fjord.

To conclude, the long-term joint distribution of parameters for wind and wave conditions in a fjord provides a condensed representation of all data from numerical simulation. It also provides the environmental basis for determining the extreme load effects for ULS and cyclic load effects for FLS, which are very useful in the design check of floating bridges. However, it should be noted that in the long-term joint distribution, the wave data only include wind-generated waves and swell is not considered.

Acknowledgment

This work was supported by the Norwegian Public Roads Administration and in parts by the Research Council of Norway through the Centre for Ships and Ocean Structures (CeSOS) and Centre for Autonomous Marine Operations and Systems (AMOS), at the Department of Marine Technology, NTNU, Trondheim, Norway. The support is gratefully acknowledged by the authors. The first author appreciates the support from the State Key Laboratory of Ocean Engineering (GKZD010075), Shanghai Jiao Tong University, Shanghai, China.

Appendix A.

Table A.6: Scatter diagram of measured significant wave height $H_{s,M}$ and the discrepancy between simulated and measured significant wave height ΔH_s from Feb. 2016 to June 2017.

$H_{s,M}\backslash\Delta H_s$	[-0.5, -0.4]	[-0.4, -0.3]	[-0.3, -0.2]	[-0.2, -0.1]	[-0.1, -0]	[0, 0.1]	[0.1, 0.2]	[0.2, 0.3]	[0.3, 0.4]	[0.4, 0.5]	[0.5, 0.6]	[0.6, 0.7]	Sum
[0, 0.1]	0	0	0	0	238	938	98	29	1	0	0	0	1304
[0.1, 0.2]	0	0	0	165	3147	1375	361	71	11	9	2	1	5142
[0.2, 0.3]	0	0	7	477	851	750	281	103	26	3	1	0	2499
[0.3, 0.4]	0	2	88	222	427	429	225	66	23	2	2	0	1486
[0.4, 0.5]	0	15	45	95	167	176	108	63	26	4	3	0	702
[0.5, 0.6]	0	7	31	30	75	88	85	51	16	3	1	0	387
[0.6, 0.7]	0	3	8	25	43	46	57	23	11	4	0	0	220
[0.7, 0.8]	0	1	1	5	19	27	22	19	7	0	0	0	101
[0.8, 0.9]	0	0	0	3	5	12	15	5	1	0	0	0	41
[0.9, 1.0]	0	0	1	2	0	5	3	1	1	1	0	0	14
[1.0, 1.1]	1	0	2	2	0	2	1	0	0	0	2	0	10
[1.1, 1.2]	0	0	0	1	0	0	0	0	0	0	0	0	1
[1.2, 1.3]	0	0	0	1	0	1	0	0	0	2	0	0	4
[1.3, 1.4]	0	0	0	0	1	0	0	0	0	0	0	0	1
[1.4, 1.5]	0	0	0	0	1	0	0	0	0	0	0	0	1
[1.5, 1.6]	0	0	0	0	0	0	0	0	0	0	0	0	0
[1.6, 1.7]	0	0	0	1	0	1	0	0	0	0	0	0	2
[1.7, 1.8]	0	1	0	0	1	0	0	0	0	0	0	0	2
Sum	1	29	183	1029	4975	3850	1256	431	123	28	11	1	11917

References

Bitner-Gregersen, E., 2012. Joint long-term models of met-ocean parameters. Marine Technology and Engineering: CENTEC Anniversary Book, C. Guedes Soares, Y. Garbatov, N. Fonseca, and A. Teixeira, eds 1, 19–34.

Bitner-Gregersen, E.M., 2005. Joint probabilistic description for combined seas, in: ASME 2005 24th International Conference on Offshore Mechanics and Arctic Engineering, American Society of Mechanical Engineers.

Bitner-Gregersen, E.M., Haver, S., 1991. Joint Environmental Model For Reliability Calculations, in: The First International Offshore and Polar Engineering Conference, International Society of Offshore and Polar Engineers, Edinburgh, The United Kingdom.

Booij, N., Ris, R.C., Holthuijsen, L.H., 1999. A third-generation wave model for coastal regions: 1. model description and validation. Journal of geophysical research: Oceans 104, 7649–7666.

Carter, D., 1982. Prediction of wave height and period for a constant wind velocity using the jonswap results. Ocean Engineering 9, 17–33.

Cheng, Z., Gao, Z., Moan, T., 2018. Hydrodynamic load modeling and analysis of a floating bridge in homogeneous wave conditions. Marine Structures 59, 122–141.

Cheng, Z., Gao, Z., Moan, T., 2019a. Numerical modeling and dynamic analysis of a floating bridge subjected to wind, wave, and current loads. Journal of Offshore Mechanics and Arctic Engineering 141, 011601.

Cheng, Z., Svangstu, E., Gao, Z., Moan, T., 2019b. Field measurements of inhomogeneous wave conditions in Bjørnafjorden. Journal of Waterway, Port, Coastal, and Ocean Engineering 145, 05018008.

Datawell, B., 2014. Datawell waverider manual DWR4.

DNV GL, 2014. Environmental Conditions and Environmental Loads (DNV-RP-C205). Det Norske Veritas AS, Oslo, Norway.

Eidem, M.E., 2017. Overview of floating bridge projects in norway, in: Proceedings of the ASME 2017 36th International Conference on Ocean, Offshore and Arctic Engineering, ASME.

Fredriksen, A.G., Heiervang, M.F., Larsen, P.N., Sandnes, P.G., Sørby, B., Bonnemaire, B., Nesteby, A., Nedrebø, Ø., 2019. Hydrodynamical aspects of pontoon optimization for a side-anchored floating bridge. Journal of Offshore Mechanics and Arctic Engineering 141, 031603.

Haver, S., 1980. Analysis of Uncertainties Related to the Stochastic Modelling of Ocean Waves. PhD thesis. Norwegian Institute of Technology.

Haver, S., Winterstein, S.R., 2009. Environmental contour lines: A method for estimating long term extremes by a short term analysis. Transactions of the Society of Naval Architects and Marine Engineers 116, 116–127.

Horn, J.T., Bitner-Gregersen, E., Krokstad, J.R., Leira, B.J., Amdahl, J., 2018. A new combination of conditional environmental distributions. Applied Ocean Research 73, 17–26.

Johannessen, K., Meling, T.S., Haver, S., 2002. Joint distribution for wind and waves in the northern north sea. International Journal of Offshore and Polar Engineering 12.

Kvåle, K.A., 2017. Dynamic behaviour of floating bridges exposed to wave excitation: A numerical and experimental investigation. PhD thesis. Norwegian University of Science and Technology.

Li, L., Gao, Z., Moan, T., 2015. Joint distribution of environmental condition at five european offshore sites for design of combined wind and wave energy devices. Journal of Offshore Mechanics and Arctic Engineering 137, 031901.

Lothe, A., Musch, O., 2015. Bjørnafjorden submerged floating tube bridge: sea state simulations. Technical Report. Norconsult AS.

Madsen, H.O., Krenk, S., Lind, N.C., 2006. Methods of structural safety. Courier Corporation.

Moan, T., Gao, Z., Ayala-Uraga, E., 2005. Uncertainty of wave-induced response of marine structures due to long-term variation of extratropical wave conditions. Marine Structures 18, 359–382.

Naess, A., Moan, T., 2013. Stochastic dynamics of marine structures. Cambridge University Press, Cambridge, UK.

NORSOK N-003, 2017. Actions and action effects. Norwegian Technology Standard, Oslo, Norway.

Skamarock, W.C., Klemp, J.B., Dudhia, J., Gill, D.O., Barker, D.M., Huang, X.Y., Wang, W., Powers, J.G., 2008. A description of the advanced research WRF version 3. Technical Report. NCAR Tech. Note NCAR/TN-475+STR. National Center For Atmospheric Research, Boulder Colorado, USA.

Tucker, M.J., Pitt, E.G., 2001. Waves in ocean engineering. Elsevier.

Watanabe, E., 2003. Floating bridges: past and present. Structural Engineering International 13, 128–132.

Winterstein, S.R., Engebretsen, K., 1998. Reliability-based prediction of design loads and responses for floating ocean structures, in: 17 th International Conference on Offshore Mechanics and Arctic Engineering, Lisbon, Portugal, p. 1998.

Winterstein, S.R., Ude, T.C., Cornell, C.A., Bjerager, P., Haver, S., 1993. Environmental parameters for extreme response: Inverse form with omission factors, in: Proceedings of the ICOSSAR-93, Innsbruck, Austria, pp. 551–557.

Xu, Y., Øiseth, O., Moan, T., Naess, A., 2018. Prediction of long-term extreme load effects due to wave and wind actions for cable-supported bridges with floating pylons. Engineering Structures 172, 321–333.